

van der Waals density functional with corrected C_6 coefficientsK. Berland,^{1,2,*} D. Chakraborty,^{3,4} and T. Thonhauser^{3,4,†}¹*Faculty of Science and Technology, Norwegian University of Life Sciences, Ås, Norway*²*Centre for Materials Science and Nanotechnology, University of Oslo, Oslo, Norway*³*Department of Physics, Wake Forest University, Winston-Salem, North Carolina 27109, USA*⁴*Center for Functional Materials, Wake Forest University, Winston-Salem, North Carolina 27109, USA*

(Received 12 February 2019; published 13 May 2019)

The nonlocal van der Waals density functional (vdW-DF) has had tremendous success since its inception in 2004 due to its constraint-based formalism that is rigorously derived from a many-body starting point. However, while vdW-DF can describe binding energies and structures for van der Waals complexes and mixed systems with good accuracy, one long-standing criticism—also since its inception—has been that the C_6 coefficients that derive from the vdW-DF framework are largely inaccurate and can be wrong by more than a factor of 2. It has long been thought that this failure to describe the C_6 coefficients is a conceptual flaw of the underlying plasmon framework used to derive vdW-DF. We prove here that this is not the case and that accurate C_6 coefficients can be obtained without sacrificing the accuracy at binding separations from a modified framework that is fully consistent with the constraints and design philosophy of the original vdW-DF formulation. Our design exploits a degree of freedom in the plasmon-dispersion model ω_q , modifying the strength of the long-range van der Waals interaction and the crossover from long to short separations, with additional parameters tuned to reference systems. Testing the new formulation for a range of different systems, we not only confirm the greatly improved description of C_6 coefficients, but we also find excellent performance for molecular dimers and other systems. The importance of this development is not necessarily that particular aspects such as C_6 coefficients or binding energies are improved, but rather that our finding opens the door for further conceptual developments of an entirely unexplored direction within the exact same constrained-based nonlocal framework that made vdW-DF so successful in the first place.

DOI: [10.1103/PhysRevB.99.195418](https://doi.org/10.1103/PhysRevB.99.195418)

I. INTRODUCTION

Materials in which van der Waals interactions, i.e., London dispersion forces, play a crucial role for cohesion and binding properties now stand at the forefront of a number of major scientific and technological advances. Examples include gas storage and filtering in supermolecular complexes and porous materials [1–3], organic electronic and optoelectronic applications [4,5], and pharmaceutical [6], ferroelectric [7,8], and photovoltaic molecular crystals [9,10]. Common to several of these developments is the increasing role of first-principles electronic-structure calculations at the density-functional theory (DFT) level—serving not only to gain insight into their functionality, but also to predict new materials and functionality prior to experimental synthesization [5]. As the ability to design and analyze materials often hinges on the ability to accurately predict energetic and structural properties, over the years great effort has been made to improve DFT. In this regard, a major development was the inclusion of van der Waals interactions by various means during the previous decade [11–24]. However, unfortunately, current methods to treat van der Waals interactions still have not achieved the same level of accuracy and reliability for such noncovalently

bonded systems as what is now typical for covalently bonded ones.

Amongst the various methods to capture van der Waals interactions within DFT, the van der Waals density functional (vdW-DF) method developed by Langreth, Lundqvist, and coworkers [14–16,25–29] stands out in that it is a true density functional, i.e., it can be evaluated from knowledge of the density alone, and employs a nonlocal correlation functional $E_c^{nl}[n]$ to account for dispersion forces. The tremendous success of vdW-DF is rooted in its plasmon dispersion formalism that is rigorously derived from a many-body starting point and adheres to a number of exact physical constraints [14,30]. This nonlocal correlation functional has since become the cornerstone of several higher-level improvements that, e.g., adjust the exchange functional that is being used in conjunction with $E_c^{nl}[n]$ [31–34]. However, despite its success and widespread use, further conceptual development of vdW-DF has come to a halt—although around the turn of the last decade, vdW-DF inspired the related and well-crafted functionals by Vydrov and Voorhis (VV) [21–24], its fundamental framework has not changed since 2004. Furthermore, one common criticism has also plagued vdW-DF for almost the same time span, i.e., the often poor C_6 coefficients that derive from it [23,27,35], which has been thought to be a conceptual flaw in the underlying framework. The poor C_6 coefficients in vdW-DF themselves bare little to no effect on the vdW-DF performance for binding energies and structures, but they are a formal shortcoming

*kristian.berland@nmbu.no

†thonhauser@wfu.edu

nonetheless. We prove here that this is not a conceptual flaw of the framework and that a modification of the underlying plasmon dispersion model corrects the C_6 coefficients and opens the door for utilizing an entirely unexplored degree of freedom that may be used for further improvements—all while adhering to the same physical constraints that made the original vdW-DF formalism so transferable and successful.

To understand which changes are necessary inside vdW-DF, we review in the next section the underlying framework but defer the reader to in-depth discussions elsewhere [14,16,26–28]. The nonlocal correlation functional $E_c^{\text{nl}}[n]$ in vdW-DF can be derived as a systematic expansion of the adiabatic connection formula (ACF) [36–38] in terms of an effective plasmon propagator S , which has poles for real frequencies at the effective plasmon frequency $\omega_{\mathbf{q}}$, where \mathbf{q} is the momentum of the plasmon. A number of exact physical constraints on S and $\omega_{\mathbf{q}}$ explain the transferability and success of vdW-DF in describing diverse classes of materials [15,16,27,39]. However, the C_6 coefficients in vdW-DF arise exclusively from the $\mathbf{q} \rightarrow 0$ limit of the plasmon dispersion $\omega_{\mathbf{q}}$, which is not constrained in vdW-DF and arises merely as a byproduct of the particular parametrization of $\omega_{\mathbf{q}}$. As a result, vdW-DF typically exhibits inferior C_6 coefficients compared to other methods.

Here, we modify the vdW-DF framework, fully consistent with the original constraints and design philosophy, but with a new and more flexible parametrization of the plasmon dispersion $\omega_{\mathbf{q}}$. This flexibility is exploited to provide accurate C_6 values, resulting in a mean absolute relative deviation (MARD) of the C_6 coefficients of 11% compared to 20% for the original formulation, which we refer to here as vdW-DF1 [14], and 56% for vdW-DF2 [25]. In addition—although not the primary purpose of this paper—the form of $\omega_{\mathbf{q}}$ is also tuned to provide noticeable improvements for binding energies of several molecular dimer systems, making the functional a contender for applications to this class of systems. Finally, the new formulation is also trivial to implement in compute codes with existing vdW-DF implementations.

II. THEORY

The nonlocal correlation in vdW-DF is given by the second-order expansion of the ACF in terms of a plasmon propagator S , describing virtual charge-density fluctuations of the electron gas, as follows:

$$E_c^{\text{nl}}[n] = \int_0^\infty \frac{du}{4\pi} \int \frac{d^3\mathbf{q}}{(2\pi)^3} \frac{d^3\mathbf{q}'}{(2\pi)^3} \times [1 - (\hat{\mathbf{q}} \cdot \hat{\mathbf{q}}')^2] S_{\mathbf{q},\mathbf{q}'}(iu) S_{\mathbf{q}',\mathbf{q}}(iu), \quad (1)$$

where S is given by

$$S_{\mathbf{q},\mathbf{q}'}(iu) = \frac{1}{2} [\tilde{S}_{\mathbf{q},\mathbf{q}'}(iu) + \tilde{S}_{\mathbf{q}',\mathbf{q}}(iu)], \quad (2)$$

$$\tilde{S}_{\mathbf{q},\mathbf{q}'}(iu) = \int d^3\mathbf{r} \frac{4\pi n(\mathbf{r}) e^{-i(\mathbf{q}-\mathbf{q}')\cdot\mathbf{r}}}{(iu + \omega_{\mathbf{q}}(\mathbf{r}))(-iu + \omega_{\mathbf{q}'}(\mathbf{r}))}. \quad (3)$$

Here, $\omega = iu$ is the imaginary frequency, $n(\mathbf{r})$ is the electron density, and $4\pi n(\mathbf{r})$ is the square of the plasmon frequency. This particular form of S as been chosen because it fulfills four

exact physical constraints [14], making vdW-DF such a powerful and transferable tool. In our modification of the method, we retain the same model of S as in earlier versions, but update the plasmon dispersion $\omega_{\mathbf{q}}(\mathbf{r}) = q^2/[2h(q/q_0(\mathbf{r}))]$ by modifying the dimensionless switching function $h(q/q_0(\mathbf{r}))$, which controls the relative strength of the density response at different length scales. The function $q_0(\mathbf{r})$ parameterizes the local response of the electron gas and is determined by the requirement that the first-order term in S in the ACF expansion reproduces a general gradient approximation-type exchange-correlation (XC) functional [16,27,30]. This XC functional, which is generally not the same as in the total energy functional, is named the *internal* functional $\epsilon_{\text{xc}}^{\text{int}}$ [14,16,40]. $q_0(\mathbf{r})$ is related to the exchange-correlation per particle through this first-order expression in S as follows:

$$\begin{aligned} \epsilon_{\text{xc}}^{\text{int}}(\mathbf{r}) &= \pi \int \frac{d^3\mathbf{q}}{(2\pi)^3} \left[\frac{1}{\omega_{\mathbf{q}}(\mathbf{r})} - \frac{2}{q^2} \right] \\ &= 2\pi \int \frac{d^3\mathbf{q}}{(2\pi)^3} \frac{1}{q^2} [h(q/q_0(\mathbf{r})) - 1] \\ &= -\frac{1}{\pi} q_0(\mathbf{r}) \int_0^\infty dy [1 - h(y)]. \end{aligned} \quad (4)$$

If we constrain the remaining integral to be

$$\int_0^\infty dy [1 - h(y)] = \frac{3}{4}, \quad (5)$$

then $q_0(\mathbf{r})$ can conveniently be expressed as a modulated Fermi wave vector $k_{\text{F}}^3(\mathbf{r}) = 3\pi^2 n(\mathbf{r})$, i.e., $q_0(\mathbf{r}) = -(4\pi/3) \epsilon_{\text{xc}}^{\text{int}}(\mathbf{r}) = (\epsilon_{\text{xc}}^{\text{int}}(\mathbf{r})/\epsilon_{\text{x}}^{\text{LDA}}(\mathbf{r})) k_{\text{F}}(\mathbf{r})$.

The vdW-DF framework dictates three constraints on $h(y)$, but also leaves considerable freedom. First, the integral over $h(y)$ should be constrained by Eq. (5). Second, a quadratic small- y limit in $h(y) = \gamma y^2 + \dots$ (where γ is a constant) ensures the appropriate C_6/r^6 long-range limit. In fact, Hyldgaard *et al.* [30] pointed out that $h(0) = 0$ corresponds to charge conservation of the spherical XC hole model of the internal functional, which is given by a Fourier transformation of $h(q/q_0(\mathbf{r}))$. Third, $h(y)$ is required to increase monotonically to a large- y limit of $\lim_{y \rightarrow \infty} h(y) = 1$, corresponding to $\omega_{\mathbf{q}} \rightarrow q^2/2$ in the limit of large q . This allows S to cancel the self-interaction divergence, i.e., the $2/q^2$ term in Eq. (4), in the ACF formula [14,39]. The standard switching function in vdW-DF1 and vdW-DF2 was chosen within these constraints as

$$h_{\text{std}}(y) = 1 - \exp(-\gamma y^2), \quad (6)$$

where the value of $\gamma = \gamma_{\text{std}} = 4\pi/9 \approx 1.3963$ is determined by Eq. (5). Note that $h_{\text{std}}(y)$ includes only one parameter, which is fully constrained.

Dispersion forces in vdW-DF can be viewed as arising from a coupling of semilocal XC holes of separated bodies [30]. For two such bodies A and B far apart, the C_6 coefficient is given by

$$C_6 = \frac{3}{\pi} \int_0^\infty du \alpha_A(iu) \alpha_B(iu), \quad (7)$$

with the far-field polarizability of body A (and likewise for B) given by

$$\alpha_A(iu) = \int_A d^3\mathbf{r} \frac{n(\mathbf{r})}{\omega_0^2(\mathbf{r}) + u^2}, \quad (8)$$

where $\omega_0(\mathbf{r}) = \lim_{q \rightarrow 0} \omega_q(\mathbf{r}) = q_0(\mathbf{r})^2/2\gamma$ for any h function with the required small- y limit from the second constraint. It is very interesting to see that the first constraint is a condition for the integral over all values of y , but the asymptotic limit that determines the C_6 coefficients is determined exclusively by the small- y limit in the second constraint. Crucially, there is significant residual freedom in the form of possible $h(y)$ functions that still fulfill all three constraints. Specifically, from the second constraint it follows that $\gamma = \lim_{y \rightarrow 0} h(y)/y^2$, which could take almost any number. Moreover, as $C_6 \propto \gamma^3$, controlling the value of γ is paramount to securing accurate C_6 values.

At the heart of our modification is a new switching function that still fulfills all three constraints, but that is also crafted to improve the description of C_6 coefficients. In particular, we propose

$$h_{\text{new}}(y) = 1 - \left(1 + \frac{(\alpha - \gamma)y^2 + A(\alpha, \gamma, \beta)y^4}{1 + A(\alpha, \gamma, \beta)y^2} \right) \exp(-\alpha y^2), \quad (9)$$

where $A(\alpha, \gamma, \beta) = (\beta + \alpha(\alpha/2 - \gamma))/(1 + \gamma - \alpha)$. This three-parameter function $h_{\text{new}}(y)$ provides significantly more freedom than $h_{\text{std}}(y)$. We get the required small- y limit of $h_{\text{new}}(y) = \gamma y^2 - \beta y^4 + \dots$, or equivalently

$$\frac{y^2}{h_{\text{new}}(y)} = \frac{1}{\gamma} + \frac{\beta}{\gamma^2} y^2 + \mathcal{O}(y^4), \quad (10)$$

which shows that—while γ controls the magnitude of the asymptote and C_6 coefficients— β/γ^2 is the leading order term determining how van der Waals interactions are reduced at shorter separations. We found the optimal values to be $\alpha = 2.01059$, $\beta = 8.17471$, and $\gamma = \gamma_{\text{new}} = 1.84981$, as described below. The functions $h_{\text{new}}(y)$ and $h_{\text{std}}(y)$ are plotted in Fig. 1 for comparison. The nonlocal correlation energy in Eq. (1) can also be written as $E_c^{\text{nl}}[n] = \frac{1}{2} \int d^3\mathbf{r} d^3\mathbf{r}' n(\mathbf{r}) \phi(\mathbf{r}, \mathbf{r}') n(\mathbf{r}')$, where the kernel $\phi(\mathbf{r}, \mathbf{r}')$ is fully determined through Eqs. (1)–(3); the two switching functions $h_{\text{new}}(y)$ and $h_{\text{std}}(y)$ result in two different kernels $\phi_{\text{new}}(\mathbf{r}, \mathbf{r}')$ and $\phi_{\text{std}}(\mathbf{r}, \mathbf{r}')$, the difference of which is plotted in Fig. S1.

The value of $\gamma_{\text{new}} = 1.84981$ was determined by minimizing the MARD of a set of 34 closed-shell atoms and small molecules compiled by VV [23]; computational details are provided in Appendix A. For a given internal functional, tuning the γ parameter corresponds to scaling the C_6 coefficients by γ^3 . Note that vdW-DF1 and vdW-DF2 use different internal functionals, as described in Appendix B. If we use the internal functional of vdW-DF2, the optimal scaling $(\gamma_{\text{new}}/\gamma_{\text{std}})^3 = 2.32529$, resulting in a MARD for the C_6 coefficients of 11.13%. If one instead tried to optimize C_6 coefficients with the vdW-DF1 internal functional, the lowest achievable MARD would be 18.56%—hence, our modified version of vdW-DF utilizes the vdW-DF2 internal functional. The value of $\beta = 8.17471$, with a corresponding

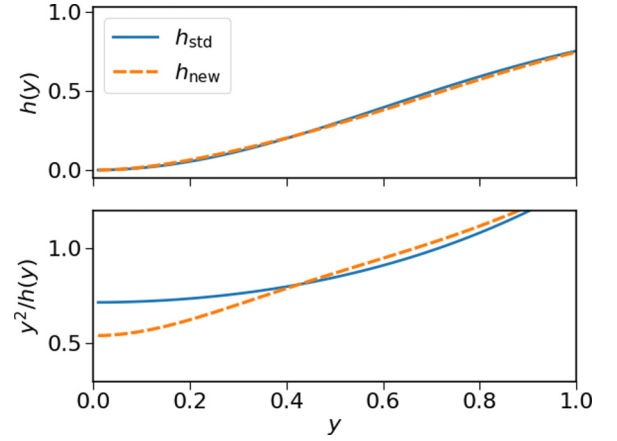


FIG. 1. Comparison of the standard switching function $h_{\text{std}}(y)$ used in vdW-DF1 and vdW-DF2 and the new switching function $h_{\text{new}}(y)$. The upper panel shows $h(y)$, while the lower panel shows $y^2/h(y)$, which is proportional to the plasmon pole ω_q . Somewhat surprisingly, the overall shape of both functions is strikingly similar, which is related to the fact that they obey the same underlying constraints. However, in the $y < 0.4$ region there are significant differences, most visible in the bottom panel.

$\alpha = 2.01059$, was determined by minimizing the MARD of the binding energies of the S22 data set with separations optimized along the center-of-mass coordinates, which results in a MARD value of 5.72%. In the optimization, for each value of β , α was adjusted to fulfill Eq. (5).

Finally, the nonlocal correlation energy from Eq. (1) has to be combined with a (semi)local functional to give the entire exchange-correlation energy $E_{\text{xc}}[n]$:

$$E_{\text{xc}}[n] = E_{\text{xc}}^{\text{sl}}[n] + E_c^{\text{nl}}[n]. \quad (11)$$

Only local density approximation (LDA) correlation is included in $E_{\text{xc}}^{\text{sl}}[n]$ as in all standard vdW-DF variants, whereas for the exchange contribution of $E_{\text{xc}}^{\text{sl}}[n]$ we employ the B86R functional of Hamada [34]. Note that our choice for the β parameter is dependent on the exchange functional employed. Since β is optimized for a reference set of systems, the binding energies are less sensitive to the exchange functional choice than in standard vdW-DF. Nonetheless, the exchange has a strong impact on binding separations [39–43]. vdW-DF variants based on soft exchange functionals, such as C09 [31], optB86b [33], and cx13 [40] have generally been found to be more versatile than those based on the harder revPBE [44] and PW86r [45] originally employed in vdW-DF1 [14] and vdW-DF2 [25]. The B86R [34] functional of Hamada was chosen because it was constructed for vdW-DF2 and we retain the same internal functional as vdW-DF2. vdW-DF2-B86R provides accurate binding separations for layered and adsorption systems, molecular dimers, and lattice constants of solids. Moreover, the B86R exchange functional goes as $s^{2/5}$ in the large- s limit, where s is the reduced gradient, which Murray *et al.* [45] argued to be a suitable choice as it avoids spurious long-range binding effects in the exchange channel. The cx13 exchange functional used in vdW-DF1-cx was not employed because this functional was originally constructed

for consistency with the internal exchange functional of vdW-DF1.

III. RESULTS

The parameters in our new switching function have been chosen to provide accurate C_6 coefficients and a low MARD for the S22 set. We first present here values for the C_6 coefficients of our new framework, followed by a systematic test of the performance of our new modification to ensure that the improved C_6 coefficients do not come at the detriment of worse performance in other areas. As such, we consider a range of standard test systems—specifically, the S66 set of molecular dimers relevant for biomolecular systems, the X40 set of halogenated molecules, and 23 solids. However, more in-depth testing, also considering challenging extended systems such as molecular crystals and surface adsorption, would be necessary if we were to release our new formulation as a general purpose functional—but that is not the intent and we merely want to show that the improved C_6 coefficients come with reasonable performance in other areas. To assess strengths and weaknesses of our modifications, we also applied a number of other commonly employed van der Waals functionals to the same systems. Details on our computational approach can be found in Appendix A. See also Supplemental Material (SM) for detailed results for all the in-

dividual systems presented in this paper [46], which includes Refs. [14,27,33,47,49,73].

A. C_6 coefficients

The improvement in C_6 values are illustrated in Fig. 2, with numerical data provided in Appendix C, for a set of 34 systems compiled by VV [23]. Figure 2 shows that—while vdW-DF2 consistently underestimates C_6 coefficients by a factor of approximately 2—their trends are far more accurately described than in vdW-DF1, which overestimates the C_6 coefficients of small molecules. This behavior is the reason for the choice of the internal functional of vdW-DF2 for our new formulation, allowing for a smaller MARD with a common scaling factor $(\gamma_{\text{new}}/\gamma_{\text{std}})^3$ that corrects the C_6 coefficients for a wide range. Overall, we find the expected improvement of the MARD value for C_6 coefficients, which now drops to 11.13% for our new formulation compared to 19.97% for vdW-DF1 and 55.64% for vdW-DF2. This value is on par with the very best of all functionals tested, i.e., 10.73% for rVV10 in Appendix C, albeit the VV formalism has been derived either by relaxing some of the original constraints of vdW-DF or, in the case of the widely employed VV10 functional [24], through heuristic rationalization.

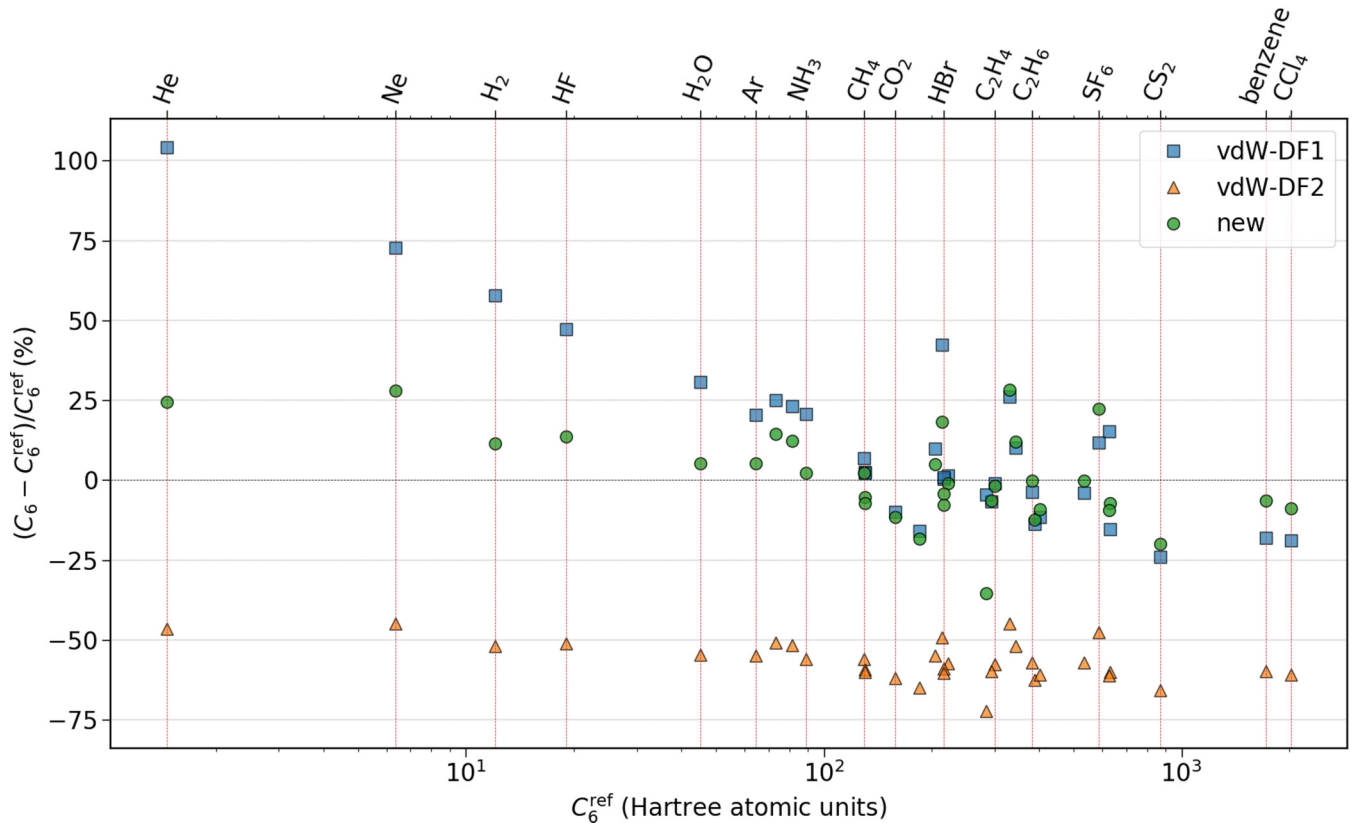


FIG. 2. Relative deviations of C_6 coefficients of vdW-DF1 (filled squares), vdW-DF2 (triangles), and our new framework (circles) for a set of 34 systems compiled by Vydrov and Voorhis, with reference data from a variety of sources [23]. The C_6 coefficients are calculated from Eqs. (7) and (8). Selected systems are labeled along the upper x axis. The corresponding MARD values are 19.97% (vdW-DF1), 55.64% (vdW-DF2), and 11.13% (new), showing the drastic improvement of C_6 values. Explicit values for all C_6 coefficients—also including other functionals for comparison—can be found in Appendix C.

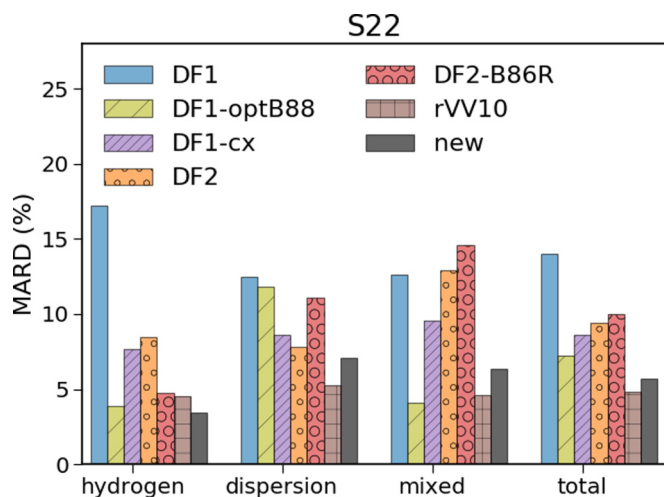


FIG. 3. MARD of the binding energy for the S22 data set, split into the characteristic hydrogen- and dispersion-bonded systems and mixtures of these bonding types.

B. Molecular dimers

1. The S22 set

Figure 3 shows the MARD of the binding energies of the S22 set of molecular dimers. More detailed data is available in Appendix C. The fact that vdW-DF1-optB88, rVV10, and our new development has a MARD smaller than $\sim 7\%$ is a result of optimizing either the exchange (in vdW-DF1-optB88) or correlation (in rVV10 and our new development) to this data set. Because of this bias, we will not further analyze the results for the S22 data set.

2. The S66 set

The S66 set of molecular dimers is larger and more diverse than the S22, featuring several dimers involving nonaromatic molecules and double-hydrogen bonds. Moreover, reference binding separations are more accurate [47].

Figure 4 shows the MARD of the binding energies of the S66 set and Appendix C provides details on their statistical properties. In addition, Fig. 5 depicts a violin plot overlaid on a box plot showing the distribution of deviations in separation (upper panel) and energy (lower panel). Overall, we find acceptable performance for binding energies for all functionals and one can see that all successor functionals indeed improve on the original vdW-DF1 functional to varying degrees. The good performance of our new formulation does carry over from the S22 data set and we find a median and mean deviation very close to zero. We note that all functionals have outliers, with the binding energy of the neopentane dimer being overestimated for all but the vdW-DF2-B86R, which, on the other hand, tends to underestimate binding energies of systems involving aromatic dimers. We also note that the MARD of the S66 set is smaller than that of S22 for all nonreference system optimized methods, i.e., vdW-DF1, vdW-DF1-cx, vdW-DF2, and vdW-DF2-B86R, as well as for our new modification, with a MARD of 4.62% compared to 5.72% for S22. For the case of vdW-DF1-optB88, the increased MARD for the S66 set compared to S22 is due

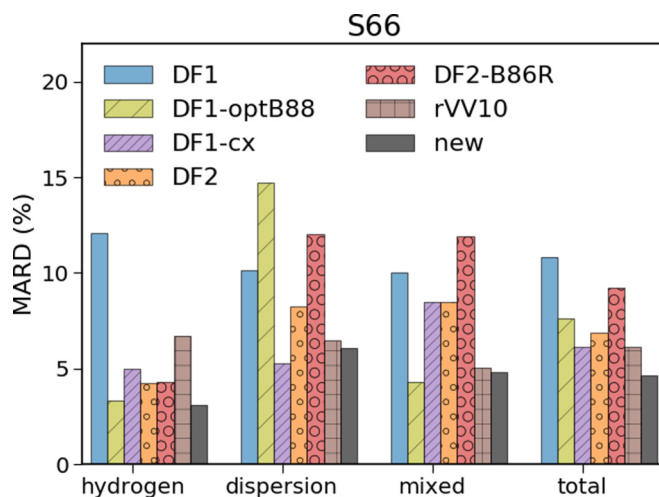


FIG. 4. MARD of the binding energy for the S66 data set, split into the characteristic hydrogen- and dispersion-bonded systems and mixtures of these bonding types.

to a reduced accuracy for dispersion-bonded systems; in particular the binding energies of dimers involving pentane and neopentane, which are not in the S22 set, are significantly overestimated. The binding energies of these dimers are also overestimated to a smaller extent with rVV10, but the reduced accuracy is also due to overestimated binding energies of double-hydrogen bonded dimers.

Looking at the upper panel of Fig. 5, we find that vdW-DF1-optB88 and rVV10 have the most accurate binding separations; however, in essence all but vdW-DF1 and vdW-DF1-cx show good separations, both of which also show a significant spread. Overestimated separations are a well-known shortcoming of vdW-DF1. The overestimation of vdW-DF1-cx stems from dimers where at least one molecule is an alkane. This result can be related to the fact that this functional was not constructed to provide accurate performance for systems with large reduced gradients s [40].

3. The X40 set

The X40 set is a set of noncovalently bonded dimers involving halogenated molecules. They span a wide variety of different bond characteristics, such as dispersion-dominated F_2 -methane binding, dipole-dipole bonds, and hydrogen and halide bonds [49]. Figure 6 shows a violin/box plot for the X40 set, with statistical data for binding energies summarized in Appendix C. The binding separations exhibit similar trends as for S66, but with decreased deviations due to the generally shorter dimer separations. Overall, we find that the binding energies of vdW-DF1-optB88 and our new formulation have the best agreement with the reference data. Like for the S66 data set, our new method follows the same trends as vdW-DF2-B86R but avoids the net underestimation of binding energies exhibited by vdW-DF2-B86R. In general, the binding energy MARD is larger for the X40 set than the S66. The rVV10 functional has the largest increase in MARD when going from the S66 to X40, from 6.19% to 15.0%. In contrast, our new modification merely increases from 4.62% to 7.06%.

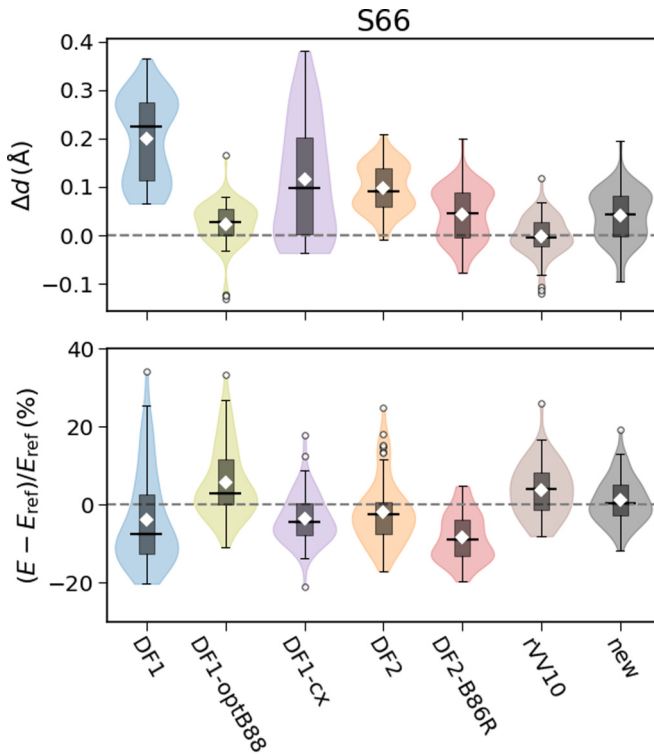


FIG. 5. Visualization (violin plot overlaid on a box plot) of the deviations from reference data of the different functionals for the S66 data set. The upper panel gives deviations in separations and the lower panel shows the relative deviation of the binding energy. The violin plots (transparent color) represent the data distribution and are based on a Gaussian kernel density estimation using the Scott’s rule [48] as implemented in MATPLOTLIB. In the box plot, the boxes hold 50% of the data, with equal number of data points above and below the median deviation (full black line). The whiskers indicate the range of data falling within $1.5 \times \text{box-length}$ beyond the upper and lower limits of the box. Outliers beyond this range are indicated with circular markers and are identified in the SM [46]. The diamonds mark the mean deviation.

C. Solids

The original vdW-DF1 and its successor vdW-DF2 both overestimated lattice constants of solids. However, combining vdW-DF correlation with soft exchange functionals with a small “PBEsol”-type enhancement factor [39,50], i.e., with a Taylor expansion of the form $F_x(s) \approx \mu_{\text{PBEsol}} s^2 + \dots$, significantly improves solid lattice constants [29,33,39,40,51,52] and, in fact, can also improve atomization energies compared to the generalized-gradient approximation [29,33].

Figure 7 shows results of our performance testing for the same set of 23 solids as considered by Klimeš *et al.* [33], with further numerical data provided in Appendix C and Tables S7 and S8 in the SM [46]. The reference data are based on zero-point corrected experimental lattice constants and atomization energies, as detailed in Ref. [33] and references therein. All the functionals with soft exchange, i.e., vdW-DF1-cx, vdW-DF2-B86R, and our new modifications, give a mean absolute deviation (MAD) for the separations of less than 0.06 Å, whereas vdW-DF2 is the least accurate. All functionals, except vdW-DF1 and vdW-DF2, also have an atomization

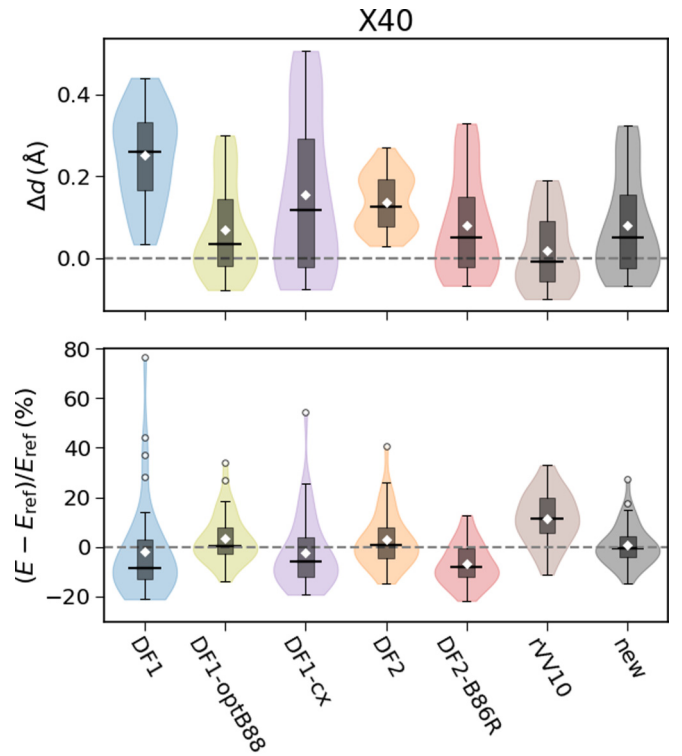


FIG. 6. Violin/box plots for deviations in separation and binding energy for the X40 set, see caption of Fig. 5 for further details.

energy MARD smaller than 5% and our new modification and rVV10 have mean and median deviations close to zero. Furthermore, as expected, our modification gives lattice constants that are similar to those of vdW-DF2-B86R, which employs the same exchange functional; atomization energies are also similar but our new formulation shows slightly improved values on average.

IV. DISCUSSION

Our study highlights the importance of the specific form of the wave-vector dependence in $\omega_{\mathbf{q}}$ through its switching function $h(y)$. In doing so, we open the door for developments around this so far unexplored degree of freedom within powerful physical constraints. Exploiting this freedom through a judicious choice of the switching function $h(y)$, we have demonstrated how accurate C_6 coefficients are fully compatible with the constraints of the original vdW-DF, which has been a major criticism of vdW-DF in general and vdW-DF2 in particular. At the same time, we exploited the fact that vdW-DF2 predicts trends in the C_6 coefficients more accurately than vdW-DF1.

We do not expect the improvement of C_6 coefficients to carry over to large nanostructures where local-field effects can be important, such as fullerenes [53–55], which would require higher-order terms in S within vdW-DF. However, at binding separations, such higher-order terms are generally less crucial, at least within vdW-DF [30,56], as multipole effects are described to second order in S . Moreover, vdW-DF includes nonadditive effects originating from changes in the electronic density [57].

Drawing attention to the possibility of adjusting $h(y)$ within vdW-DF introduces a measure of flexibility that so far has been missing in standard vdW-DF. In fact, since the release of vdW-DF1 in 2004 [14], a number of exchange functionals have been proposed that aim both to improve binding energies and remedy the notorious overestimation of binding separations present in vdW-DF1 and to some extent in vdW-DF2. This practice has recently been criticized [58] as the large exchange term is fitted to match the smaller nonlocal correlation term; colloquially, the “tail wags the dog.” Two extreme cases of such a practice are (i) the Bayesian-error-estimation-vdW functional (BEEF-vdW) [59], in which machine learning was used to determine a semilocal exchange functional for the vdW-DF2 nonlocal correlation employing diverse training sets and (ii) the vdW-DF1-cx functional [40], in which the exchange was designed to be formally as consistent with the vdW-DF1 nonlocal correlation as feasible. Because of its flexibility, VV10 (or rVV10) has seen many adaptations both to different semilocal XC functionals and to different benchmark sets [58,60–63]. The vdW-DF flexibility is more limited than that of VV10 both because of the constraints inherent to the method and the fact that the exchange functional must still be a good match with the semilocal correlation description of vdW-DF, which gives a strong preference for “soft” exchange functionals [39,50].

In our new formulation, we optimized the parameters of the proposed $h_{\text{new}}(y)$ not only to improve the C_6 coefficients but also to improve the binding energies of the S22 set of molecular dimers. This improvement carries over to accurate molecular binding properties of the S66 set and the X40 set. With the choice of B86R, our new formulation also provides accurate lattice constants for solids. While the performance on molecular dimers is encouraging, we emphasize that our new proposed switching function is not necessarily the very best choice for a versatile performance for different classes of systems as our focus was on improving C_6 coefficients and the S22 set of molecular dimers was used to adjust the plasmon model. As a simple test on different classes of systems, we also studied adsorption of small molecules in metal organic frameworks and on surfaces. In particular, for CO_2 adsorption in MOF-74, our binding energy shows a 20% overestimation of experiment compared to DF1: 8%, DF1-optB88: 26%, DF1-cx: 14%, DF2: 6%, DF2-B86R: 4%, and rVV10: 16%. For the case of benzene on the Au(111) surface, we also find a significant overestimation of binding energy of 22%, compared to DF1: -20% , DF1-optb88: 10%, DF1-cx: 9%, DF2: -23% , DF2-b86R: -7% , and rVV10: 15%. Although these are challenging systems, these tests indicate that there is still room for improvement of our new formulation. We thus fully expect that new and potentially better forms of $h(y)$ with significant performance increase over a wide array of systems will be developed by us or others in the near future and enjoy widespread usage. For this reason, we do not give our modified formulation a new name or number within the lineup of vdW-DF1 and vdW-DF2 functionals.

V. SUMMARY

We present a reformulation of the plasmon model that underpins the popular vdW-DF exchange-correlation func-

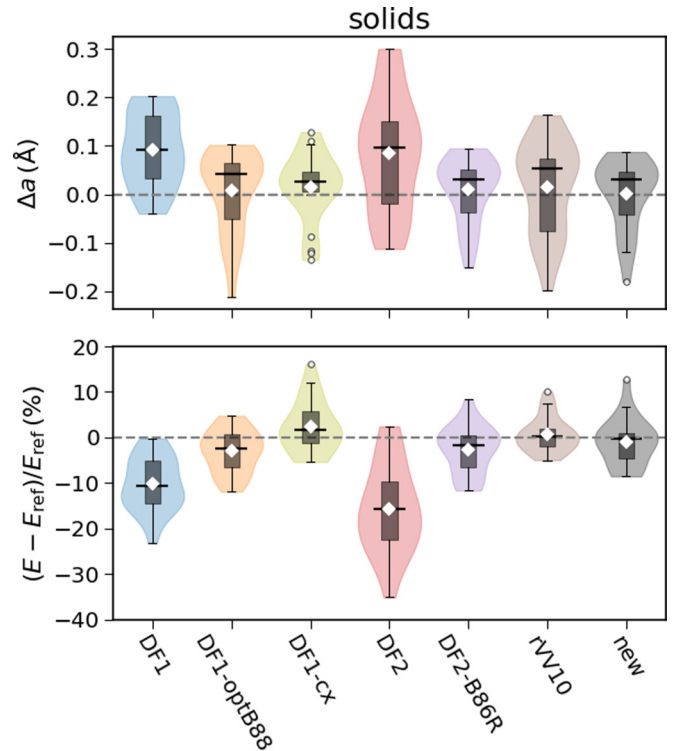


FIG. 7. Violin/box plots for deviations in lattice constants a and atomization energies of a set of 23 solids, see Tables S7 and S8 for further numerical details and see caption of Fig. 5 for a description of violin and box plots.

tional. Our reformulation is entirely within the constraint-based framework of the original vdW-DF and thus inherits its good transferability. Our formulation takes advantage of some freedom concerning the choice of a switching function that connects two constrained limits. We use this additional freedom to correct a long-standing criticism of vdW-DF, i.e., the often wrong C_6 coefficients that derive from it. Our work thus proves that this formal shortcoming is not an inherent flaw of the vdW-DF formalism, but merely the byproduct of a particular choice in its parametrization. We test our updated formalism and find the expected improvement in the C_6 coefficients, but we also find good overall performance with regard to binding energies and separations for a range of systems. While we have used this previously unexplored degree of freedom to improve the C_6 coefficients, we see the main importance of our work in that this freedom may also be used for further conceptual developments of vdW-DF and improvements of other properties.

ACKNOWLEDGMENTS

K.B. thanks Per Hyldgaard for discussions. Work in Norway was supported by the Research Council of Norway Project No. 250346 and ancillary support from UiO Energy. All work in the US was entirely supported by NSF Grant No. DMR-1712425.

APPENDIX A: COMPUTATIONAL DETAILS

Our new vdW-DF formulation has been implemented in—and all our calculations have been performed with—the QUANTUM ESPRESSO package [64]. The C_6 coefficients were calculated directly from Eqs. (7) and (8). For all our calculations, we have used the PBE GBRV ultrasoft pseudopotentials due to their excellent transferability [65]. However, that database did not include potentials for He, Ne, Ar, and Kr; for those elements, we used the standard PBE RRKJ ultrasoft potentials provided by QUANTUM ESPRESSO. In all calculations, the wave function and density cutoff were ~ 680 eV (50 Ryd) and ~ 8200 eV (600 Ryd), respectively. We used an energy convergence criterion of $\sim 1.36 \times 10^{-5}$ eV (1×10^{-6} Ryd) for molecular systems and $\sim 1.36 \times 10^{-7}$ eV (1×10^{-8} Ryd) for solids. For metals and semiconductors, a Gaussian smearing was used with a broadening of ~ 0.1 eV (0.00735 Ryd). Lattice parameters and cohesive energies of solids were determined from the Birch-Murnaghan equation of state [66,67]. For comparison and to assess the performance of our new formulation, we performed calculations with the following exchange-correlation functionals: vdW-DF (also called vdW-DF1 here) [14], vdW-DF1-optB88 [32], vdW-DF1-cx [40], vdW-DF2 [25], vdW-DF2-B86R [34], and rVV10 [24,68]. The corresponding short names we may use in tables and figures are DF1, DF1-optB88, DF1-cx, DF2, DF2-B86R, and rVV10, respectively.

For the various molecular dimer data sets (S22 [69], S66 [47], X40 [49]), calculations were performed at the Γ -point with molecules in a box surrounded by at least 15 Å of vacuum to minimize spurious interactions with periodic replica. To test the performance of a given functional on a given data set, we followed commonly accepted procedures for those data sets. In particular, the monomers were considered frozen and a fixed number of geometries—representing different separations—were generated by moving one monomer along an axis specified through the optimal structure provided by

that data set. For the S22 data set, a center-of-mass axis was used as suggested by Molner *et al.* [70]; for the S66 and X40 data sets, an “interaction coordinate” was used as suggested in the corresponding original works [47,49]. Single point calculations were then performed on those geometries to generate binding energy curves, from which we extracted the binding energy minima and binding separations through fitting to a Lagrange polynomial near the minimum.

We have considered 23 solids, semiconductors, and ionic salts as listed in Klimeš *et al.* [32]. Periodic solids have been calculated with a k -point mesh of $15 \times 15 \times 15$ for cubic systems and $10 \times 10 \times 10$ for hexagonal/tetragonal systems. To calculate the atomization energies, individual atoms have been calculated in a box with at least 15 Å of vacuum.

APPENDIX B: THE INTERNAL FUNCTIONAL $\epsilon_{xc}^{\text{int}}$

In vdW-DF1 [14], the internal functional is given by the LDA XC energy with Langreth-Vosko exchange gradient corrections for a slowly varying electron gas [71], whereas in vdW-DF2 [25] gradient corrections are given by the large- N asymptote of neutral atoms [72]. In both cases, it takes the form

$$\epsilon_{xc}^{\text{int}}(\mathbf{r}) = \epsilon_c^{\text{LDA}}(\mathbf{r}) + \epsilon_x^{\text{LDA}}(\mathbf{r})[1 - (Z_{ab}/9)s(\mathbf{r})^2], \quad (\text{B1})$$

with $Z_{ab} = -0.8491$ in vdW-DF1 and -1.8867 in vdW-DF2. For our modification, we employ the same large- N limit for the internal functional as vdW-DF2 because in our construction it results in more accurate C_6 coefficients than the internal functional of vdW-DF1.

APPENDIX C: DATA

Statistical data supporting the figures are provided in Tables I–V. Detailed data on individual systems are provided in the SM [46].

TABLE I. C_6 coefficients [Hartree atomic units] for a set of 34 closed-shell atoms and small molecules compiled by Vydrov and Voorhis [23]. The C_6 coefficients are calculated from Eqs. (7) and (8). For each data set, we give the mean deviation (MD), mean absolute deviation (MAD), mean relative deviation (MRD), and mean absolute relative deviation (MARD). The first three data sets (vdW-DF1, vdW-DF1-optB88, vdW-DF1-cx) all share the same nonlocal vdW-DF1 kernel and only differ in their choice of exchange—thus, their results are very close to each other and the small differences are a measure of the effect of exchange on the C_6 coefficients. Similarly, the next two data sets (vdW-DF2 and vdW-DF2-B86R) both use the vdW-DF2 kernel (with different exchanges) and produce very comparable results.

	vdW-DF1	vdW-DF1-optB88	vdW-DF1-cx	vdW-DF2	vdW-DF2-B86R	rVV10	new	Ref.
He	2.98	2.94	3.09	0.76	0.78	1.45	1.82	1.46
Ne	10.96	10.35	10.85	3.92	3.50	8.44	8.13	6.35
Ar	77.63	74.94	75.99	30.38	29.16	70.08	67.81	64.42
Kr	132.9	128.1	128.7	54.97	51.92	131.2	120.8	130.1
Be	304.6	296.7	310.3	106.4	108.9	186.0	253.1	214
Mg	723.0	671.5	727.6	246.9	243.9	425.0	568.0	627
Zn	271.6	244.3	256.3	79.23	78.66	163.0	183.3	284
H ₂	19.07	18.87	20.07	5.59	5.81	10.28	13.49	12.09
N ₂	91.92	89.32	91.02	37.48	36.16	88.70	84.07	73.43
Cl ₂	335.9	325.8	325.1	154.1	146.6	366.7	341.0	389.2
HF	27.99	27.00	27.80	9.59	9.28	21.13	21.59	19.00

TABLE I. (Continued.)

	vdW-DF1	vdW-DF1-optB88	vdW-DF1-cx	vdW-DF2	vdW-DF2-B86R	rVV10	new	Ref.
HCl	133.6	129.8	131.4	54.88	53.19	124.6	123.7	130.4
HBr	218.4	209.9	212.5	91.89	85.78	200.2	199.6	216.6
CO	100.3	97.71	99.69	40.24	39.32	93.51	91.42	81.40
CO ₂	143.1	139.6	141.0	62.52	60.39	159.4	140.4	158.7
CS ₂	661.8	643.7	645.0	310.9	299.7	739.4	697.1	871.1
OCS	356.0	346.6	348.2	163.0	157.2	395.6	365.5	402.2
N ₂ O	155.7	151.4	153.1	66.93	64.86	172.4	150.8	184.9
CH ₄	138.5	136.5	141.1	56.11	56.98	129.6	132.4	129.6
CCl ₄	1644	1600	1592	828.7	792.8	2044	1844	2024
NH ₃	107.6	103.8	108.1	39.99	39.22	82.78	91.19	89.03
H ₂ O	59.24	57.08	58.94	21.21	20.52	44.95	47.72	45.29
SiH ₄	379.2	374.6	388.5	162.2	165.7	344.6	385.0	343.9
SiF ₄	416.2	404.7	408.1	187.0	182.1	455.8	423.5	330.2
H ₂ S	217.7	211.9	215.8	90.59	89.21	200.3	207.4	216.8
SO ₂	274.8	266.5	268.5	123.5	118.5	305.2	275.6	294.0
SF ₆	655.3	634.9	635.3	319.5	307.9	869.9	716.3	585.8
C ₂ H ₂	224.6	218.5	223.3	94.02	92.22	210.3	214.4	204.1
C ₂ H ₄	297.4	291.0	298.1	127.4	127.0	297.3	295.1	300.2
C ₂ H ₆	367.4	362.3	372.0	162.1	163.9	396.6	380.9	381.8
CH ₃ OH	225.5	220.7	226.3	94.96	94.50	226.1	219.7	222.0
CH ₃ OCH ₃	513.3	505.1	518.4	228.5	229.6	567.9	533.7	534.0
C ₃ H ₆	534.9	527.6	538.6	250.6	251.6	632.6	584.8	630.8
C ₆ H ₆	1411	1385	1403	701.5	694.0	1838	1614	1723
MD	-20.23	-29.80	-24.05	-203.3	-206.5	2.42	-15.41	—
MAD	51.06	52.87	53.92	203.3	206.5	36.20	38.11	—
MRD [%]	11.36	8.02	10.91	-55.64	-56.58	1.24	0.97	—
MARD [%]	19.97	19.10	20.72	55.64	56.58	10.73	11.13	—

TABLE II. Statistical analysis of the performance of various van der Waals functionals for the binding energies of the S22 set, see Tables S1 and S2 for details.

	vdW-DF1	vdW-DF1-optB88	vdW-DF1-cx	vdW-DF2	vdW-DF2-B86R	rVV10	new
<i>Hydrogen bonded</i>							
MD [meV]	103	14.7	34.9	58.0	25.1	-21.4	14.9
MAD [meV]	103	15.7	34.9	58.0	25.1	21.4	15.9
MRD [%]	-17.2	-3.75	-7.67	-8.50	-4.72	4.50	-3.30
MARD [%]	17.2	3.88	7.67	8.50	4.72	4.50	3.43
<i>Dispersion bonded</i>							
MD [meV]	3.98	-20.4	3.95	8.17	20.5	2.98	-9.76
MAD [meV]	15.8	22.4	10.9	13.0	20.5	7.28	12.7
MRD [%]	9.26	9.95	3.82	2.88	-11.9	-1.54	3.43
MARD [%]	13.5	13.0	9.66	8.26	11.9	4.73	7.98
<i>Mixed</i>							
MD [meV]	22.2	4.74	16.4	21.1	23.3	6.53	10.4
MAD [meV]	23.0	6.70	16.5	21.9	23.3	8.29	10.4
MRD [%]	-10.2	-1.88	-8.16	-10.4	-13.2	-2.63	-5.40
MARD [%]	11.4	3.89	8.24	11.7	13.2	5.31	5.42
<i>Full set</i>							
MD [meV]	41.4	-1.24	17.8	28.2	22.9	-3.64	4.49
MAD [meV]	46.0	15.3	20.3	30.2	22.9	12.1	13.0
MRD [%]	-5.35	1.83	-3.65	-4.97	-10.0	0.04	-1.52
MARD [%]	14.0	7.19	8.58	9.42	10.0	4.84	5.72

TABLE III. Statistical analysis of the performance of various van der Waals functionals for the binding energies of the S66 set, see Table S3 and S4 for details.

	vdW-DF1	vdW-DF1-optB88	vdW-DF1-cx	vdW-DF2	vdW-DF2-B86R	rVV10	new
<i>Hydrogen bonded</i>							
MD [meV]	51.4	-1.47	14.6	19.9	6.92	-25.0	-0.45
MAD [meV]	51.4	8.50	17.4	20.6	13.1	25.0	9.11
MRD [%]	-12.4	0.39	-4.34	-3.81	-2.00	7.06	0.10
MARD [%]	12.4	2.58	5.22	4.25	3.85	7.06	2.69
<i>Dispersion bonded</i>							
MD [meV]	-6.46	-20.9	2.02	-1.38	19.0	-2.50	-7.66
MAD [meV]	13.0	20.9	7.71	10.6	19.0	7.84	8.06
MRD [%]	8.11	15.6	0.77	4.22	-11.7	4.08	6.13
MARD [%]	10.4	15.6	5.12	7.82	11.7	6.21	6.39
<i>Mixed</i>							
MD [meV]	13.7	-0.83	13.1	11.8	19.3	0.98	6.08
MAD [meV]	16.3	6.24	13.5	14.0	19.3	7.87	7.54
MRD [%]	-7.70	0.63	-8.10	-6.70	-12.3	-0.46	-3.79
MARD [%]	9.83	4.15	8.49	8.60	12.3	5.15	4.80
<i>Full set</i>							
MD [meV]	19.8	-8.05	9.75	10.0	14.9	-9.29	-0.99
MAD [meV]	27.4	12.1	12.9	15.1	17.0	13.8	8.27
MRD [%]	-3.83	5.78	-3.71	-1.90	-8.51	3.74	1.02
MARD [%]	10.9	7.61	6.18	6.81	9.16	6.19	4.62

TABLE IV. Statistical analysis of the performance of various van der Waals functionals for the binding energies of the X40 set; see Tables S5 and S6 for details.

	vdW-DF1	vdW-DF1-optB88	vdW-DF1-cx	vdW-DF2	vdW-DF2-B86R	rVV10	new
MD [meV]	13.5	-6.74	2.41	2.47	3.99	-18.1	-4.53
MAD [meV]	19.9	10.4	14.1	9.86	11.9	19.2	9.46
MRD [%]	-0.12	3.93	-0.95	5.11	-5.93	13.4	1.86
MARD [%]	15.6	7.79	12.4	10.2	9.90	15.0	7.06

TABLE V. Statistical analysis of the performance of various van der Waals functionals for the lattice constants and atomization energies of a set of 23 solids assembled by Klimeš *et al.* [33].

	vdW-DF1	vdW-DF1-optB88	vdW-DF1-cx	vdW-DF2	vdW-DF2-B86R	rVV10	new
<i>Lattice constants</i>							
MD [Å]	0.09	0.01	0.01	0.09	0.01	0.02	0.002
MAD [Å]	0.10	0.07	0.06	0.12	0.06	0.09	0.06
MRD [%]	2.01	0.29	0.35	1.99	0.28	0.49	0.12
MARD [%]	2.12	1.43	1.13	2.71	1.14	1.77	1.15
<i>Atomization energies</i>							
MD [eV]	-0.32	-0.04	0.12	-0.45	-0.01	0.02	0.04
MAD [eV]	0.32	0.10	0.16	0.47	0.10	0.08	0.11
MRD [%]	-10.3	-2.81	2.82	-15.8	-2.33	0.93	-0.52
MARD [%]	10.3	4.31	4.87	16.2	4.35	2.99	4.08

- [1] K. Tan, S. Zuluaga, E. Fuentes, E. C. Mattson, J.-F. Veyan, H. Wang, J. Li, T. Thonhauser, and Y. J. Chabal, *Nat. Commun.* **7**, 13871 (2016).
- [2] H. Wang, X. Dong, J. Lin, S. J. Teat, S. Jensen, J. Cure, E. V. Alexandrov, Q. Xia, K. Tan, Q. Wang, D. H. Olson, D. M. Proserpio, Y. J. Chabal, T. Thonhauser, J. Sun, Y. Han, and J. Li, *Nat. Commun.* **9**, 1745 (2018).
- [3] B. Li, X. Dong, H. Wang, D. Ma, K. Tan, S. Jensen, B. J. Deibert, J. Butler, J. Cure, Z. Shi, T. Thonhauser, Y. J. Chabal, Y. Han, and J. Li, *Nat. Commun.* **8**, 485 (2017).
- [4] P. J. Diemer, J. Hayes, E. Welchman, R. Hallani, S. J. Pookpanratana, C. A. Hacker, C. A. Richter, J. E. Anthony, T. Thonhauser, and O. D. Jurchescu, *Adv. Electron. Mater.* **3**, 1600294 (2017).
- [5] R. Gomez-Bombarelli, J. Aguilera-Iparraguirre, T. D. Hirzel, D. Duvenaud, D. Maclaurin, M. A. Blood-Forsythe, H. S. Chae, M. Einzinger, D.-G. Ha, T. Wu, G. Markopoulos, S. Jeon, H. Kang, H. Miyazaki, M. Numata, S. Kim, W. Huang, S. I. Hong, M. Baldo, R. P. Adams, and A. Aspuru-Guzik, *Nat. Mater.* **15**, 1120 (2016).
- [6] A. M. Reilly and A. Tkatchenko, *Phys. Rev. Lett.* **113**, 055701 (2014).
- [7] K. Lee, B. Kolb, T. Thonhauser, D. Vanderbilt, and D. C. Langreth, *Phys. Rev. B* **86**, 104102 (2012).
- [8] S. Ishibashi, S. Horiuchi, and R. Kumai, *Phys. Rev. B* **97**, 184102 (2018).
- [9] L. Kronik and A. Tkatchenko, *Acc. Chem. Res.* **47**, 3208 (2014).
- [10] T. Rangel, K. Berland, S. Sharifzadeh, F. Brown-Altwater, K. Lee, P. Hyldgaard, L. Kronik, and J. B. Neaton, *Phys. Rev. B* **93**, 115206 (2016).
- [11] S. Grimme, *J. Comput. Chem.* **25**, 1463 (2004).
- [12] S. Grimme, J. Antony, T. Schwabe, and C. Mück-Lichtenfeld, *Org. Biomol. Chem.* **5**, 741 (2007).
- [13] S. Grimme, *Wiley Interdiscip. Rev. Comput. Mol. Sci.* **1**, 211 (2011).
- [14] M. Dion, H. Rydberg, E. Schröder, D. C. Langreth, and B. I. Lundqvist, *Phys. Rev. Lett.* **92**, 246401 (2004).
- [15] D. C. Langreth, B. I. Lundqvist, S. D. Chakarova-Käck, V. R. Cooper, M. Dion, P. Hyldgaard, A. Kelkkanen, J. Kleis, L. Kong, S. Li, P. G. Moses, E. D. Murray, A. Puzder, H. Rydberg, E. Schröder, and T. Thonhauser, *J. Phys. Condens. Matter* **21**, 084203 (2009).
- [16] K. Berland, V. R. Cooper, K. Lee, E. Schröder, T. Thonhauser, P. Hyldgaard, and B. I. Lundqvist, *Rep. Prog. Phys.* **78**, 066501 (2015).
- [17] A. Tkatchenko and M. Scheffler, *Phys. Rev. Lett.* **102**, 073005 (2009).
- [18] A. Tkatchenko, R. A. DiStasio, R. Car, and M. Scheffler, *Phys. Rev. Lett.* **108**, 236402 (2012).
- [19] A. Ambrosetti, A. M. Reilly, R. A. DiStasio, and A. Tkatchenko, *J. Chem. Phys.* **140**, 18A508 (2014).
- [20] A. Ambrosetti, N. Ferri, R. A. DiStasio, and A. Tkatchenko, *Science* **351**, 1171 (2016).
- [21] O. A. Vydrov and T. Van Voorhis, *J. Chem. Phys.* **130**, 104105 (2009).
- [22] O. A. Vydrov and T. Van Voorhis, *Phys. Rev. Lett.* **103**, 063004 (2009).
- [23] O. A. Vydrov and T. Van Voorhis, *Phys. Rev. A* **81**, 062708 (2010).
- [24] O. A. Vydrov and T. Van Voorhis, *J. Chem. Phys.* **133**, 244103 (2010).
- [25] K. Lee, E. D. Murray, L. Kong, B. I. Lundqvist, and D. C. Langreth, *Phys. Rev. B* **82**, 081101(R) (2010).
- [26] T. Thonhauser, V. R. Cooper, S. Li, A. Puzder, P. Hyldgaard, and D. C. Langreth, *Phys. Rev. B* **76**, 125112 (2007).
- [27] E. Schröder, V. R. Cooper, K. Berland, B. I. Lundqvist, P. Hyldgaard, and T. Thonhauser, in *Non-covalent Interactions in Quantum Chemistry and Physics: Theory and Applications*, edited by A. O. de la Roza and G. A. DiLabio (Elsevier, Amsterdam, 2017), Chap. 8, pp. 241–274.
- [28] T. Thonhauser, S. Zuluaga, C. A. Arter, K. Berland, E. Schröder, and P. Hyldgaard, *Phys. Rev. Lett.* **115**, 136402 (2015).
- [29] K. Berland, Y. Jiao, J.-H. Lee, T. Rangel, J. B. Neaton, and P. Hyldgaard, *J. Chem. Phys.* **146**, 234106 (2017).
- [30] P. Hyldgaard, K. Berland, and E. Schröder, *Phys. Rev. B* **90**, 075148 (2014).
- [31] V. R. Cooper, *Phys. Rev. B* **81**, 161104(R) (2010).
- [32] J. Klimeš, D. R. Bowler, and A. Michaelides, *J. Phys. Condens. Matter* **22**, 022201 (2010).
- [33] J. Klimeš, D. R. Bowler, and A. Michaelides, *Phys. Rev. B* **83**, 195131 (2011).
- [34] I. Hamada, *Phys. Rev. B* **89**, 121103(R) (2014).
- [35] L. M. Woods, D. A. R. Dalvit, A. Tkatchenko, P. Rodriguez-Lopez, A. W. Rodriguez, and R. Podgornik, *Rev. Mod. Phys.* **88**, 045003 (2016).
- [36] O. Gunnarsson and B. I. Lundqvist, *Phys. Rev. B* **13**, 4274 (1976).
- [37] D. C. Langreth and J. P. Perdew, *Solid State Commun.* **17**, 1425 (1975).
- [38] D. C. Langreth and J. P. Perdew, *Phys. Rev. B* **15**, 2884 (1977).
- [39] K. Berland, C. A. Arter, V. R. Cooper, K. Lee, B. I. Lundqvist, E. Schröder, T. Thonhauser, and P. Hyldgaard, *J. Chem. Phys.* **140**, 18A539 (2014).
- [40] K. Berland and P. Hyldgaard, *Phys. Rev. B* **89**, 035412 (2014).
- [41] E. Londero and E. Schröder, *Comput. Phys. Commun.* **182**, 1805 (2011).
- [42] K. Berland, Ø. Borck, and P. Hyldgaard, *Comp. Phys. Commun.* **182**, 1800 (2011).
- [43] K. Berland and P. Hyldgaard, *Phys. Rev. B* **87**, 205421 (2013).
- [44] Y. Zhang and W. Yang, *Phys. Rev. Lett.* **80**, 890 (1998).
- [45] E. D. Murray, K. Lee, and D. C. Langreth, *J. Chem. Theory Comput.* **5**, 2754 (2009).
- [46] See Supplemental Material at <http://link.aps.org/supplemental/10.1103/PhysRevB.99.195418> which includes Refs. [14,27,33,47,49,73].
- [47] J. Řezáč, K. E. Riley, and P. Hobza, *J. Chem. Theory Comput.* **7**, 2427 (2011).
- [48] D. W. Scott, *Biometrika* **66**, 605 (1979).
- [49] J. Řezáč, K. E. Riley, and P. Hobza, *J. Chem. Theory Comput.* **8**, 4285 (2012).
- [50] J. P. Perdew, A. Ruzsinszky, G. I. Csonka, O. A. Vydrov, G. E. Scuseria, L. A. Constantin, X. Zhou, and K. Burke, *Phys. Rev. Lett.* **100**, 136406 (2008).
- [51] S. F. Yuk, K. C. Pitike, S. M. Nakhmanson, M. Eisenbach, Y. W. Li, and V. R. Cooper, *Sci. Rep.* **7**, 43482 (2017).

- [52] L. Gharaee, P. Erhart, and P. Hyldgaard, *Phys. Rev. B* **95**, 085147 (2017).
- [53] E. Hult, H. Rydberg, B. I. Lundqvist, and D. C. Langreth, *Phys. Rev. B* **59**, 4708 (1999).
- [54] A. Ruzsinszky, J. P. Perdew, J. Tao, G. I. Csonka, and J. M. Pitarke, *Phys. Rev. Lett.* **109**, 233203 (2012).
- [55] J. Tao, Y. Mo, G. Tian, and A. Ruzsinszky, *Phys. Rev. B* **94**, 085126 (2016).
- [56] J. Tao, Y. Jiao, Y. Mo, Z.-H. Yang, J.-X. Zhu, P. Hyldgaard, and J. P. Perdew, *Phys. Rev. B* **97**, 155143 (2018).
- [57] Y. Jiao, E. Schröder, and P. Hyldgaard, *Phys. Rev. B* **97**, 085115 (2018).
- [58] H. Peng, Z.-H. Yang, J. P. Perdew, and J. Sun, *Phys. Rev. X* **6**, 041005 (2016).
- [59] J. Wellendorff, K. T. Lundgaard, A. Møgelhøj, V. Petzold, D. D. Landis, J. K. Nørskov, T. Bligaard, and K. W. Jacobsen, *Phys. Rev. B* **85**, 235149 (2012).
- [60] T. Björkman, *Phys. Rev. B* **86**, 165109 (2012).
- [61] A. V. Terentjev, L. A. Constantin, and J. M. Pitarke, *Phys. Rev. B* **98**, 214108 (2018).
- [62] N. Mardirossian and M. Head-Gordon, *J. Chem. Phys.* **144**, 214110 (2016).
- [63] A. Terentjevs, P. Cortona, L. Constantin, J. M. Pitarke, F. Della Sala, and E. Fabiano, *Computation* **6**, 7 (2018).
- [64] P. Giannozzi, O. Andreussi, T. Brumme, O. Bunau, M. Buongiorno Nardelli, M. Calandra, R. Car, C. Cavazzoni, D. Ceresoli, M. Cococcioni, N. Colonna, I. Carnimeo, A. Dal Corso, S. de Gironcoli, P. Delugas, R. A. DiStasio, A. Ferretti, A. Floris, G. Fratesi, G. Fugallo, R. Gebauer, U. Gerstmann, F. Giustino, T. Gorni, J. Jia, M. Kawamura, H.-Y. Ko, A. Kokalj, E. Küçükbenli, M. Lazzeri, M. Marsili, N. Marzari, F. Mauri, N. L. Nguyen, H.-V. Nguyen, A. Otero-de-la Roza, L. Paulatto, S. Poncé, D. Rocca, R. Sabatini, B. Santra, M. Schlipf, A. P. Seitsonen, A. Smogunov, I. Timrov, T. Thonhauser, P. Umari, N. Vast, X. Wu, and S. Baroni, *J. Phys. Condens. Matter* **29**, 465901 (2017).
- [65] K. F. Garrity, J. W. Bennett, K. M. Rabe, and D. Vanderbilt, *Comput. Mater. Sci.* **81**, 446 (2014).
- [66] F. Birch, *Phys. Rev.* **71**, 809 (1947).
- [67] F. D. Murnaghan, *Proc. Natl. Acad. Sci.* **30**, 244 (1944).
- [68] R. Sabatini, T. Gorni, and S. de Gironcoli, *Phys. Rev. B* **87**, 041108(R) (2013).
- [69] P. Jurecka, J. Sponer, J. Cerny, and P. Hobza, *Phys. Chem. Chem. Phys.* **8**, 1985 (2006).
- [70] L. F. Molnar, X. He, B. Wang, and K. M. Merz, *J. Chem. Phys.* **131**, 065102 (2009).
- [71] D. C. Langreth and S. H. Vosko, *Phys. Rev. Lett.* **59**, 497 (1987).
- [72] J. Schwinger, *Phys. Rev. A* **24**, 2353 (1981).
- [73] T. Takatani, E. G. Hohenstein, M. Malagoli, M. S. Marshall, and C. D. Sherrill, *J. Chem. Phys.* **132**, 144104 (2010).